



## Insights into extinction evolution during extreme low visibility events: Case study of Shanghai, China



Zhen Cheng<sup>a,b</sup>, Shuxiao Wang<sup>b,c,\*</sup>, Liping Qiao<sup>d,e</sup>, Hongli Wang<sup>d,e,\*\*</sup>, Min Zhou<sup>d,e</sup>, Xiao Fu<sup>b</sup>, Shengrong Lou<sup>d,e</sup>, Lina Luo<sup>a</sup>, Jingkun Jiang<sup>b,c</sup>, Changhong Chen<sup>d,e</sup>, Xiaoliang Wang<sup>f</sup>, Jiming Hao<sup>b,c</sup>

<sup>a</sup> School of Environmental Science and Engineering, Shanghai Jiao Tong University, Shanghai 200240, China

<sup>b</sup> State Key Joint Laboratory of Environment Simulation and Pollution Control, School of Environment, Tsinghua University, Beijing 100084, China

<sup>c</sup> State Environmental Protection Key Laboratory of Sources and Control of Air Pollution Complex, Beijing 100084, China

<sup>d</sup> Shanghai Academy of Environmental Sciences, Shanghai 200233, China

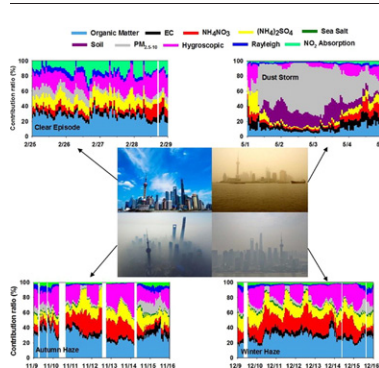
<sup>e</sup> State Environmental Protection Key Laboratory of the Cause and Prevention of Urban Air Pollution Complex, Shanghai 200233, China

<sup>f</sup> Division of Atmospheric Sciences, Desert Research Institute, 2215 Raggio Parkway, Reno, NV 89512, USA

### HIGHLIGHTS

- Hourly-resolution apportionment of ambient extinction coefficient was conducted.
- PM<sub>2.5</sub> soil and coarse particles dominated extinction coefficient during dust storm.
- RH caused the differences of contributors during autumn and winter events.

### GRAPHICAL ABSTRACT



### ARTICLE INFO

#### Article history:

Received 26 July 2017

Accepted 19 August 2017

Available online 21 October 2017

Editor: D. Barcelo

#### Keywords:

Haze

Extinction coefficient

IMPROVE algorithm

Low visibility

Shanghai megacity

### ABSTRACT

Apportionment of ambient extinction coefficient is essential for quantifying the causes of visibility degradation. Previous studies focused on either seasonal or episode-average extinction coefficients. The extinction evolution during different types of low visibility events was still unclear and seldom investigated. In this study, hourly-resolution apportionment of ambient extinction coefficient, including dry extinction coefficient and hygroscopic portion, during three low visibility events (i.e., dust storm, autumn and winter haze) and one clear episode was retrieved through online measurement in Shanghai, China. PM<sub>2.5</sub> soil and coarse particles contributed 90% of PM<sub>10</sub> mass and 62% of total extinction coefficient throughout the dust storm event. Secondary inorganic aerosol and organic matter dominated the autumn and winter haze events, accounting for 52% and 31% of PM<sub>2.5</sub> mass, 35% and 27% of extinction coefficient, respectively. Hygroscopic enhancement by inorganic particles contributed another 22–27% of extinction coefficient during the two haze events. However, higher relative humidity elevated the extinction percentage of inorganic aerosol and hygroscopic enhancement during the autumn haze, and the percentage of organic matter decreased correspondingly. In contrast, the extinction of each contributor increased proportionally and the percentages could keep at a stable level during the winter haze. Furthermore, the mass extinction efficiency of major PM<sub>2.5</sub> chemical components was found to increase with the accumulation of mass loading. These findings indicated the importance of reducing the mass level of organic matter and secondary inorganic aerosol during the

\* Correspondence to: S. Wang, State Key Joint Laboratory of Environment Simulation and Pollution Control, School of Environment, Tsinghua University, Beijing 100084, China.

\*\* Correspondence to: H. Wang, Shanghai Academy of Environmental Sciences, Shanghai 200233, China.

E-mail addresses: [shxwang@tsinghua.edu.cn](mailto:shxwang@tsinghua.edu.cn) (S. Wang), [wanghl@saes.sh.cn](mailto:wanghl@saes.sh.cn) (H. Wang).

autumn or winter haze events. The control of precursors of sulfur and nitrogen oxides seemed more effective for visibility improvement during the autumn events with higher relative humidity.

© 2017 Elsevier B.V. All rights reserved.

## 1. Introduction

Ambient fine particulate matter (PM<sub>2.5</sub>) causes horizontal visibility degradation and vertical change of radiative balance through its light extinction effect (Charlson et al., 1992; Watson, 2002). Severe problems of air pollution and radiative forcing will be deduced when PM<sub>2.5</sub> concentration exceed the threshold of ambient capacity (Bates et al., 2006; Pui et al., 2014). Various PM<sub>2.5</sub> chemical components are verified to have different levels of extinction efficiencies (Hand and Malm, 2007; Pitchford et al., 2007). Tracking the extinction apportionment from major PM<sub>2.5</sub> components will help to quantify the causes of visibility degradation and estimate aerosol radiative forcing accurately, which will in turn help the policy makers design effective strategies to improve visibility and address climate change.

The frequent and severe haze pollution in urban China has drawn global attentions as the aerosol concentration and extinction coefficient could be several times as that of clear episodes (Guo et al., 2014; Huang et al., 2014; Li and Zhang, 2014; Tian et al., 2016). Previous studies on the apportionment of extinction coefficient in urban China have been reported intensively. Annual or seasonal average of extinction apportionment were investigated through offline-filter samples at the city of Xi'an, Tianjin, Shanghai, Nanjing and Guangzhou (Cao et al., 2012; Han et al., 2012; Lin et al., 2014; Shen et al., 2014; Tao et al., 2014). As to the studies based on online measurement of super site, Han et al. (2015) compared the extinction contribution by aerosol species between haze days and non-haze days at Shanghai. Tian et al. (2016) also presented the apportionment differences between the days of 20% best visibility and 20% worst visibility at Suzhou. Wang et al. (2015) investigated the extinction contribution of each aerosol species during the nonheating and heating periods by an Aerosol Chemical Speciation Monitor at Beijing. However, seasonal or episode-average results were not sufficient for the evolution process of these extreme low visibility events. Dominant contributors and formation mechanisms might vary with different types of low visibility events. Insights into extinction evolution during different typical low visibility events were seldom reported. Furthermore, only dry ambient extinction coefficient was concerned in the above studies, which only accounting for ~46% of total extinction coefficient (Cheng et al., 2017).

In this study, three typical low visibility events, i.e., dust storm, autumn haze and winter haze, as well as one clear episode were identified and compared based on a one-year online observation campaign in Shanghai, the largest megacity of China. In-situ measurements of aerosol chemical components, ambient visibility and meteorological factors were conducted firstly. Hourly-resolution apportionments of ambient extinction coefficient, including dry extinction coefficient and hygroscopic portion, were retrieved for the above four events then. The distinct characteristics of extinction apportionment findings in this study are expected to enrich the knowledge of evolution towards visibility impairment, as well as efficient strategies towards visibility improvement for these extreme events.

## 2. Methodology

### 2.1. Observation site and events time

The observation site was located at the top of main building in Shanghai Academy of Environmental Sciences (121.43°E, 31.17°N), near the inner ring of Shanghai megacity. Shanghai is the largest megacity of China with a permanent population of more than 24 million in the year of 2014 (<http://www.stats-sh.gov.cn>). It lies in eastern of China as the

core city of the Yangtze River Delta city cluster. Its total energy consumption reached 114 million tons equivalent of coal, accompanying an annual PM<sub>2.5</sub> concentration of 52 µg/m<sup>3</sup> in the year of 2014 (<http://www.stats-sh.gov.cn>). As shown in Fig. 1, the observation site was in a typical residential and commercial area. There were no major industrial or fugitive dust sources nearby. The site was 130 m north to Caobao Road, and 650 m west to Humin Elevated Road. The sampling height was 15 m above ground level and 23 m above mean sea level.

Shanghai is dominated by the north subtropical monsoon climate, and the seasonal distribution of pollution episodes is significant. Haze events usually occur in the autumn or winter season due to the more stable meteorological dispersion conditions than other seasons (Fu et al., 2016; Hua et al., 2015; Zhou et al., 2012, 2016a, 2016b). In addition, dust storms transported from the northwest China can affect Shanghai during spring season (Fu et al., 2010; Fu et al., 2014; Li et al., 2014). Hence a one-year online observation campaign was conducted from April 1, 2011 to March 30, 2012. Three low visibility events were identified and selected for this study, including a dust storm event in spring (5/1 0:00–5/5 0:00, 2011), an autumn haze event (11/9 0:00–11/16 0:00, 2011) and a winter haze event (12/9 0:00–12/16 0:00, 2011). Meanwhile, a clear episode (2/25 16:00–2/29 16:00, 2012) with high level of visibility was selected for the comparison.

### 2.2. Online measurement instruments and models

Table 1 summarized the ambient datasets measured or modeled in this study, including PM mass concentration and major chemical components, NO<sub>2</sub> mass concentration and meteorological factors. In detail, PM<sub>2.5</sub> and PM<sub>10</sub> mass concentrations were measured by β-ray attenuation with 5-minute resolution. PM<sub>2.5</sub> water-soluble ions including sulfate (SO<sub>4</sub><sup>2-</sup>), nitrate (NO<sub>3</sub><sup>-</sup>), ammonium (NH<sub>4</sub><sup>+</sup>) and chloride (Cl<sup>-</sup>) were measured using a Monitor for Aerosols and Gases in Ambient Air (MARGA) with 1-hour resolution. PM<sub>2.5</sub> organic carbon (OC) and elemental carbon (EC) were measured by a Semi-Continuous OC-EC Field Analyzer with 30-minute resolution. Ambient relative humidity (RH) and wind speed were measured by a Met One Station with 5-minute resolution. All the above online measurement results were then averaged to hourly resolution.

Hourly concentrations of crustal elements of Al, Si, Ca, Fe and Ti were retrieved from the simulation results at the period of the four events with the model of U.S. EPA Community Modeling and Analysis System (CMAQ). Details of the CMAQ model configuration and input datasets such as emission inventory and meteorological data were described in the previous studies of our group (Fu et al., 2014, 2016). Meanwhile, mixing layer height and precipitation data with the resolution of 3-h were obtained from the Global Data Assimilation System (GDAS) model (Rolph, 2013). The records of mixing layer height corresponded to the instantaneous value of indicated time, while precipitation record was the cumulative results for 3 h.

Table 1 Instruments and their time resolution for real-time measurements used in the field campaign.

### 2.3. Data processing

Hourly PM<sub>2.5</sub> mass was reconstructed by eight sets of aerosol species according to the US IMPROVE algorithms (Watson, 2002; Pitchford et al., 2007). Concentrations of ammonium sulfate, ammonium nitrate and sea salt were estimated by multiplying MARGA reported sulfate, nitrate and chloride concentrations by factors of 1.375, 1.29, and 1.8,

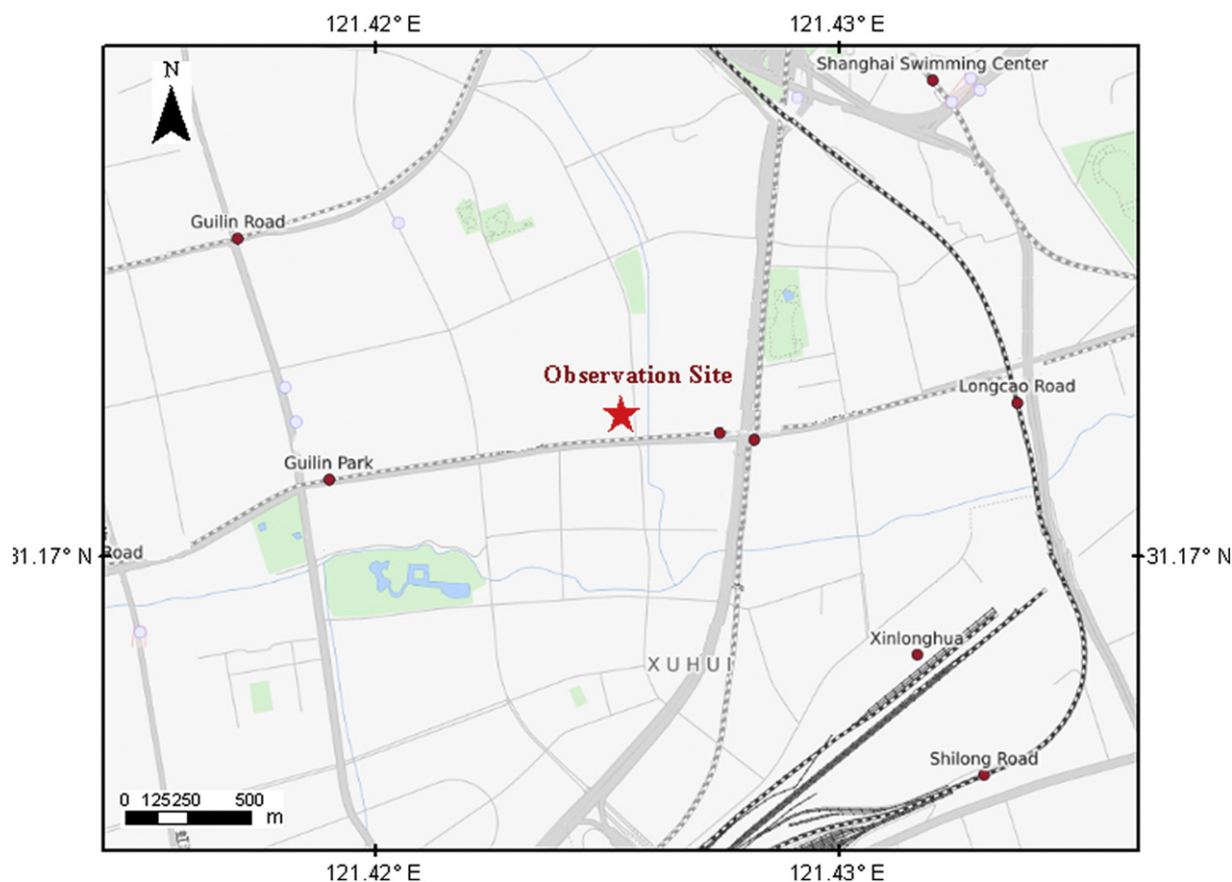


Fig. 1. Geographic location of the observation site and its surrounding area. The observation site is labeled by the red pentagram.

respectively (Pitchford et al., 2007). The neutralization status of ammonium was investigated by the comparison between the measured ammonium concentration and simulated ammonium concentration under two scenarios, i.e.,  $\text{NH}_4\text{NO}_3 + (\text{NH}_4)_2\text{SO}_4$  and  $\text{NH}_4\text{NO}_3 + \text{NH}_4\text{HSO}_4$ . From the results of Fig. 2, almost all the points located at the 1:1 line were attributed to the form of  $\text{NH}_4\text{NO}_3 + (\text{NH}_4)_2\text{SO}_4$ , indicating the forms of ammonium were ammonia sulfate but not ammonium bisulfate during all the four events.  $\text{PM}_{2.5}$  elemental carbon (EC) concentrations were determined directly by the Sunset Carbon Analyzer.  $\text{PM}_{2.5}$  organic matter (OM) concentrations were estimated by multiplying the Sunset Carbon Analyzer reported OC concentrations by a factor of 1.8 suggested by the revised IMPROVE algorithm (Pitchford et al., 2007).  $\text{PM}_{2.5}$  soil concentrations were reconstructed using the weighted summary concentration of crustal elements ( $2.2 \cdot [\text{Al}] + 2.49 \cdot [\text{Si}] + 1.63 \cdot [\text{Ca}] + 2.42 \cdot [\text{Fe}] + 1.94 \cdot [\text{Ti}]$ ) (Chow et al., 2015). The hourly concentrations of related crustal elements were derived from CMAQ simulations of the corresponding  $4 \times 4$  km grid enclosing the supersite. The difference between the directly measured  $\text{PM}_{2.5}$  mass and the sum of the above six components was regarded as “ $\text{PM}_{2.5}$

unidentified”. Coarse PM concentrations were estimated by the difference between  $\text{PM}_{10}$  and  $\text{PM}_{2.5}$  mass concentrations.

The revised IMPROVE algorithm was evaluated and applied for the hourly apportionment of extinction coefficient (Pitchford et al., 2007). The most important improvement of the revised IMPROVE algorithm over the original one is the design of small- and large-sized fractions for the components of sulfate, nitrate, and organic matter. Previous studies have suggested that the revised IMPROVE algorithm could better reproduce the measured peak of extinction coefficient than the original algorithm during the pollution episodes in China (Bian, 2011; Cheng et al., 2015; Jung et al., 2009). Ten sets of contributors were then apportioned for the ambient total extinction coefficient: Rayleigh scattering was set to a constant value of  $10 \text{ Mm}^{-1}$ ; Absorption extinction of gaseous pollutants was calculated by 0.33 multiplying ambient  $\text{NO}_2$  volume concentration (ppb); The contributions of the coarse particles and the six  $\text{PM}_{2.5}$  components of OM, EC, ammonium sulfate, ammonium nitrate, sea salt and soil, respectively were estimated according to the revised IMPROVE algorithm strictly (Pitchford et al., 2007). The last contribution of hygroscopic enhancement was estimated by the summed difference of

Table 1

Instruments and their temporal resolution for real-time measurements used in the field campaign.

Catalog	Measured parameter (unit)	Instrument (manufacturer)	Temporal resolution
Particulate matter	$\text{PM}_{2.5}$ inorganic ( $\text{SO}_4^{2-}$ , $\text{NO}_3^-$ , $\text{NH}_4^+$ , $\text{Cl}^-$ ) ( $\mu\text{g}/\text{m}^3$ )	MARGA ADI 2080 (Applikon Analytical, the Netherlands)	1 h
	$\text{PM}_{2.5}$ carbonaceous (OC, EC) ( $\mu\text{g}/\text{m}^3$ )	RT4 carbon analyzer (Sunset Laboratory, Inc., OR, USA)	30 min
	$\text{PM}_{2.5}$ and $\text{PM}_{10}$ integrated mass ( $\mu\text{g}/\text{m}^3$ )	FH62 C-14 $\beta$ -ray (50 °C heating) (Thermo Scientific Co., MA, USA)	5 min
	$\text{PM}_{2.5}$ crustal elements (Al, Si, Ca, Fe and Ti) ( $\mu\text{g}/\text{m}^3$ )	WRF3.6 + CMAQ5.0 modeling	1 h
Met factors	Visual range (m)	Model 6000 visibility sensor (Belfort Instrument, MA, USA)	5 min
	Relative humidity (%), Wind speed (m/s)	Met one station (Met One Co., OR, USA)	5 min
	Precipitation (mm), mixing layer height (m)	Global data assimilation system (GDAS) model	3 h
Gas	$\text{NO}_2$ mass ( $\mu\text{g}/\text{m}^3$ )	EC9841 (Ecotech Co., Australia)	5 min

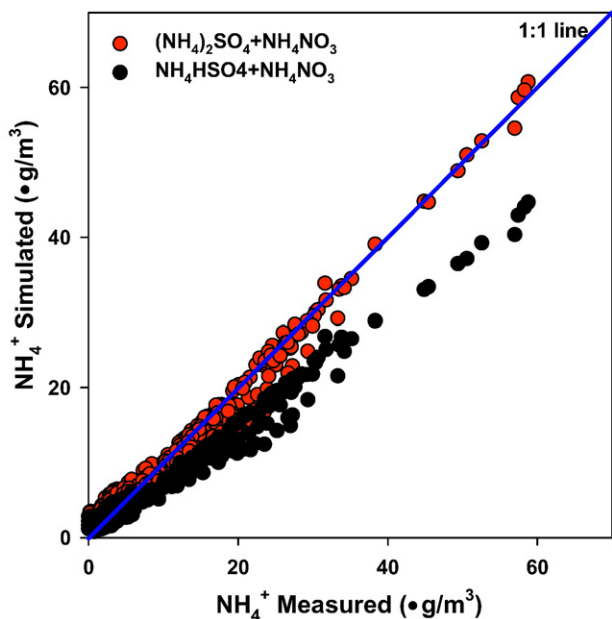


Fig. 2. Ammonium balance evaluation for the measured values during the three low visibility events and one clear episode.

extinction between ambient relative humidity and dry condition for water-soluble components, i.e., ammonium sulfate, ammonium nitrate and sea salt.

### 3. Results and discussion

#### 3.1. Characteristics of typical low visibility events

The average ambient visibility of the selected four events were  $10.8 \pm 4.8$  km for dust storm,  $20.7 \pm 16.3$  km for autumn haze,  $16.9 \pm$

$12.9$  km for winter haze and  $29.9 \pm 8.7$  km for clear episode. Although the average visibility of two haze events were better than that of dust storm, their corresponding minimum hourly visibility were 0.92 and 2.95 km, much lower than 5.73 of dust storm and 11.9 km of clear episode. Meanwhile, the counting hours with the average visibility lower than 5 km were 27 and 22 hours for autumn and winter haze, respectively, comparing with 0 hour for dust storm and clear episode. Fig. 4(a) described the variation of ambient visibility during the evolution of the four events.

#### 3.1.1. Meteorological conditions

Meteorological indicators of mixing layer height (MLH), wind speed, relative humidity and precipitation amount during the evolution of the four events were compared and shown in Fig. 3. The higher level of MLH and wind speed usually represents the better dispersion conditions for pollutants. The event-average wind speed and MLH were 2.03 m/s and 363 m for dust storm, both lower than 2.09 m/s and 577 m for autumn haze, and 2.08 m/s and 670 m for winter haze. Clear episode held the highest value of 2.35 m/s for wind speed and 799 m for MLH. However, the temporal variation of wind speed and MLH showed high consistency during the autumn, winter haze and clear episode while it is not the case during dust storm. Wind speed and MLH during the autumn and winter events both decreased to a minimum value and then recovered to the normal level. The minimum hourly wind speeds were as low as 0.68 and 0.74 m/s during the autumn and winter haze, respectively, and the corresponding MLHs were 95 m and 144 m. The peak hazy period with most unfavorable dispersion conditions occurred on November 12–13 during the autumn haze, and December 13–14 during the winter haze. In contrast, the winds speed kept higher than 2 m/s on May 1 and 2, then decrease to 1–2 m/s from May 3 during the episode of dust storm. Mixing layer depth exhibited similar diurnal pattern as wind speed, but with a different day-to-day trend from that of wind speed. The observation site was impacted by both large-scale cyclone benefit for horizontal dust transport and local-scale stable condition benefit for vertical dust accumulation. The meteorological conditions of the three low visibility events were moderate compared with

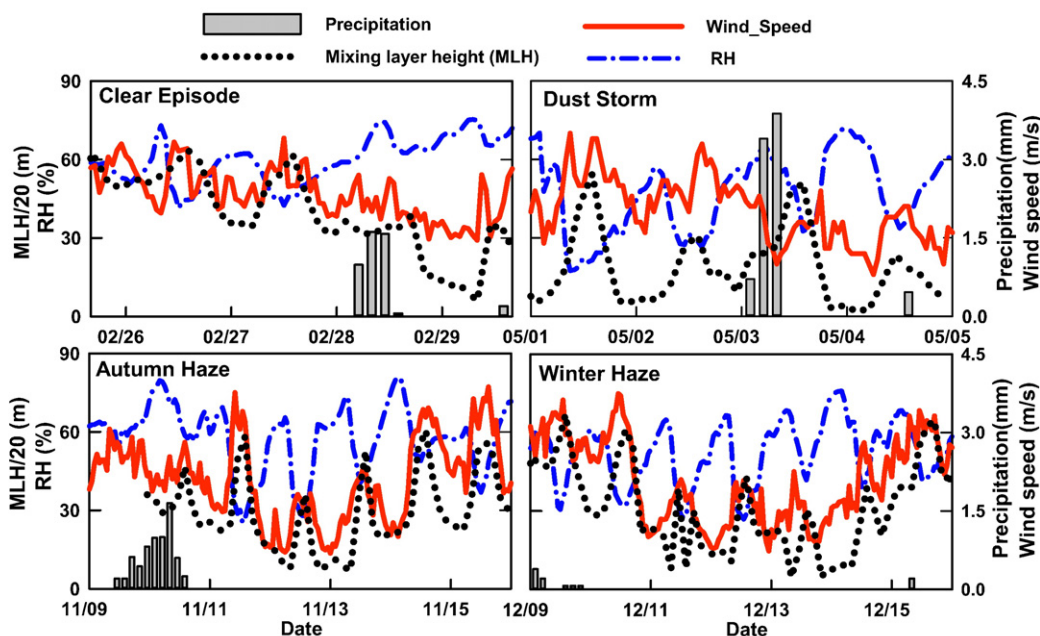


Fig. 3. Meteorological conditions during the three low visibility events and one clear episode. Red solid line represents wind speed, the black dotted line represents mixing layer height (MLH), the blue dash-dot line represents relative humidity (RH), and the gray bar represents 3-h accumulated amount of precipitation.

previous reported low visibility events. The minimum hourly wind speeds of the haze events occurred at the winter of 2007, 2012, 2013 and the autumn of 2010 are all lower than 1 m/s, with the lowest value of 0.6 m/s during January of 2013 (Fu et al., 2008; Zhou et al., 2012, 2016a, 2016b). Meanwhile, the average of 2.35 m/s during the above dust storm event was also falling in the range of 2–3 m/s, reported in another dust storm influenced Shanghai in the spring of 2007 (Fu et al., 2010).

Ambient relative humidity (RH) and precipitation amount also have important potential influence on the extent of pollution episode. The episode-average RH was 57.7% of the autumn event, higher than 46.9% of the dust storm event and 52.3% of the winter event, but lower than 59.7% of the clear episode (shown in Fig. 3). RH showed typical diurnal variation pattern in all four events due to that of ambient temperature. However, the RH during the autumn event reached as high as 81% on November 10 and 79% on November 14, potentially providing adequate moistures for aqueous reaction and fog formation. Maximum hourly RH values of 87–92% are reported during the episodes of autumn or winter haze in 2007, 2010, 2012 and 2013, even higher than the RH level in this study (Fu et al., 2008; Zhou et al., 2012, 2016a, 2016b). Generally, the RH in autumn is regarded as higher than that in winter, mostly due to the abundant moisture content brought by the southeast monsoon in summer and autumn (Zhou et al., 2012, 2016a, 2016b). The precipitation during all the four episodes was weak, only 3 mm was detected on the morning of May 3 and 1.5 mm on the night of November 10 and February 28. The limited amount of precipitation had almost negligible impact on the extinction coefficient through the direct extinction of ambient water-drop, especially during the pollution peak periods of the four events.

### 3.1.2. Aerosol chemical composition

Various characteristics of PM composition were observed during the three low visibility events and the clear episode (shown in Fig. 4). For the clear episode, the absolute mass concentration of all major PM<sub>2.5</sub> species and coarse particles keep at a low level continuously during the whole episode. Accordingly, their mass ratio varied in a stable and narrow range throughout the episode. Specifically, organic matter, ammonia sulfate and ammonia nitrate contributed 26%, 19% and 11% to the integrated PM<sub>2.5</sub> mass of 30.5 µg/m<sup>3</sup>, respectively. Coarse particles contributed 16.4 µg/m<sup>3</sup> (35%) of PM<sub>10</sub> mass during the clear episode. For the dust storm event, PM<sub>2.5</sub> soil and coarse particles dominated the PM<sub>10</sub> mass during the dust storm. The average concentrations of PM<sub>2.5</sub> soil and coarse particles during dust storm reached as high as 80 and 393 µg/m<sup>3</sup>, accounting for 15% and 75% of total PM<sub>10</sub> mass concentration, respectively. The PM<sub>10</sub> size distribution and PM<sub>2.5</sub> chemical compositions further illustrated that the source of dust storm event was transported from the long-distance dust. In detail, the dust storm reached the observation site in the morning of May 1. The peak period of this event with hourly PM<sub>10</sub> concentration higher than 400 µg/m<sup>3</sup> lasted from the noon of May 1 to the night of May 3, then decreased continually. The peak PM<sub>10</sub> concentration of 999 µg/m<sup>3</sup> occurred at 15:00 of May 2, while the maximum level of soil in PM<sub>2.5</sub> was 166 µg/m<sup>3</sup> and occurred on the morning of May 3.

Carbonaceous substances and secondary inorganic aerosol (SIA) in PM<sub>2.5</sub> were dominant during the two haze events, but a bit different influenced by relative humidity between autumn and winter haze. Concentration of SIA was 55 and 50 µg/m<sup>3</sup> for autumn and winter haze, respectively, along with ~32 µg/m<sup>3</sup> of organic matter. They together contributed 79–87% of PM<sub>2.5</sub> and the mass ratio of PM<sub>2.5</sub>/PM<sub>10</sub> was 61–76% during the autumn and winter haze. PM<sub>2.5</sub> mass in the autumn event increased rapidly from the night of November 10, consistent with the decrease of wind speed and MLH. The peak time with the lowest wind speed and MLH occurred on the morning of November 13, while the maximum PM<sub>2.5</sub> mass of 439 µg/m<sup>3</sup> occurred at 23:00 of November 13. This delay was likely due to the higher RH in the night of November 13, which triggered dense fog and enhanced the aqueous reaction for

SIA. This hypothesis was supported by the PM<sub>2.5</sub> compositions during the peak hours. Ammonium sulfate and ammonium nitrate increased from ~50 µg/m<sup>3</sup> to 126 and 114 µg/m<sup>3</sup>, respectively in several hours before the peak hour. Organic matter also reached as high as 122 µg/m<sup>3</sup>, but with a lower increase rate compared to SIA. Accordingly, the mass percentage of organic matter decreased continuously from ~30% to ~17% throughout the autumn haze, while that of SIA increased from ~15% at the beginning to 30–53% until the peak pollution hour, then decreased quickly with the pollution dissipation. Unlike the autumn haze, the mass accumulation of major PM<sub>2.5</sub> components kept synchronous and consistent during the entire winter haze. PM<sub>2.5</sub> mass started to accumulate with the decrease of wind speed and MLH from December 10. The peak pollution period lasted from the night of December 13 to the morning of December 15 with a maximum hourly PM<sub>2.5</sub> value of 251 µg/m<sup>3</sup>. The mass percentage of major PM<sub>2.5</sub> components varied in a stable range during the entire winter event, i.e., 13–29% for organic matter, 11–27% for ammonium sulfate and 11–28% for ammonium nitrate. In summary, the mass percentage and temporal variation of PM<sub>2.5</sub> components indicated that the winter event was primarily driven by the accumulation of primary and secondary particles under unfavorable dispersion conditions. The higher ratio of secondary inorganic aerosol in autumn haze could be attributed to the high relative humidity which could enhance the aqueous formation path of SIA.

## 3.2. Chemical apportionment of extinction coefficient

### 3.2.1. Performance evaluation of the IMPROVE algorithm

Firstly the hourly actual extinction coefficient (at the wavelength of 550nm) was converted from the measured ambient visibility according to Koschmieder's formula ( $b_{\text{ext}} \cdot \text{Mm}^{-1} = 3912/\text{visibility\_km}$ ) (Larson and Gass, 1989). Then the reconstructed extinction coefficient by the IMPROVE algorithm was compared with it during the four episodes. As shown in Fig. 5, the reconstructed extinction coefficient could repeat the observed values during the evolution of four events. The temporal trend and absolute value agreed well between the two datasets. The results of chemical extinction contribution based on the IMPROVE algorithm were reasonable and believable. However, significant overestimation by the IMPROVE algorithm during some peak episodes of haze events were also observed. For the autumn and winter haze events, the IMPROVE reconstructed extinction coefficients were 29% higher than the measured in average, mostly caused by the bias during the hours of pollution peak. For the clear and dust storm events, the IMPROVE reconstructed values were only 13% higher than the measured with the R square of 0.92. As a result, the IMPROVE algorithm overestimate the actual extinction coefficient by 27% in average for all the four events. The phenomenon of overestimation by the revised IMPROVE algorithm was also reported by other studies in China. Our another observation in 2012 in Shanghai found that 12% of dry scattering extinction coefficient was overestimated by the revised IMPROVE algorithm (Cheng et al., 2015). From the measurement results of Guangzhou, another megacity of China, overestimation of dry scattering extinction coefficient was 51% in summer (Jung et al., 2009) and 3% in winter for the revised IMPROVE algorithm (Tao et al., 2012). The most possible cause of the overestimation phenomenon was the cut-off concentration of 20 µg/m<sup>3</sup> used for the small and large model split, making the higher MSE percentage falling into the large mode in China. This will be discussed in Section 3.3 further.

### 3.3. Chemical extinction contribution during different events

The above four events exhibited different levels of extinction coefficient, as well as major contributors (shown in Fig. 6). For the clear episode, the total extinction coefficient was only  $189 \pm 68 \text{ Mm}^{-1}$ . The largest five contributors were organic matter of 26%, hygroscopic enhancement of 20%, ammonium sulfate of 13%, NO<sub>2</sub> absorption of 13% and ammonium nitrate of 8%. The chemical extinction contributions

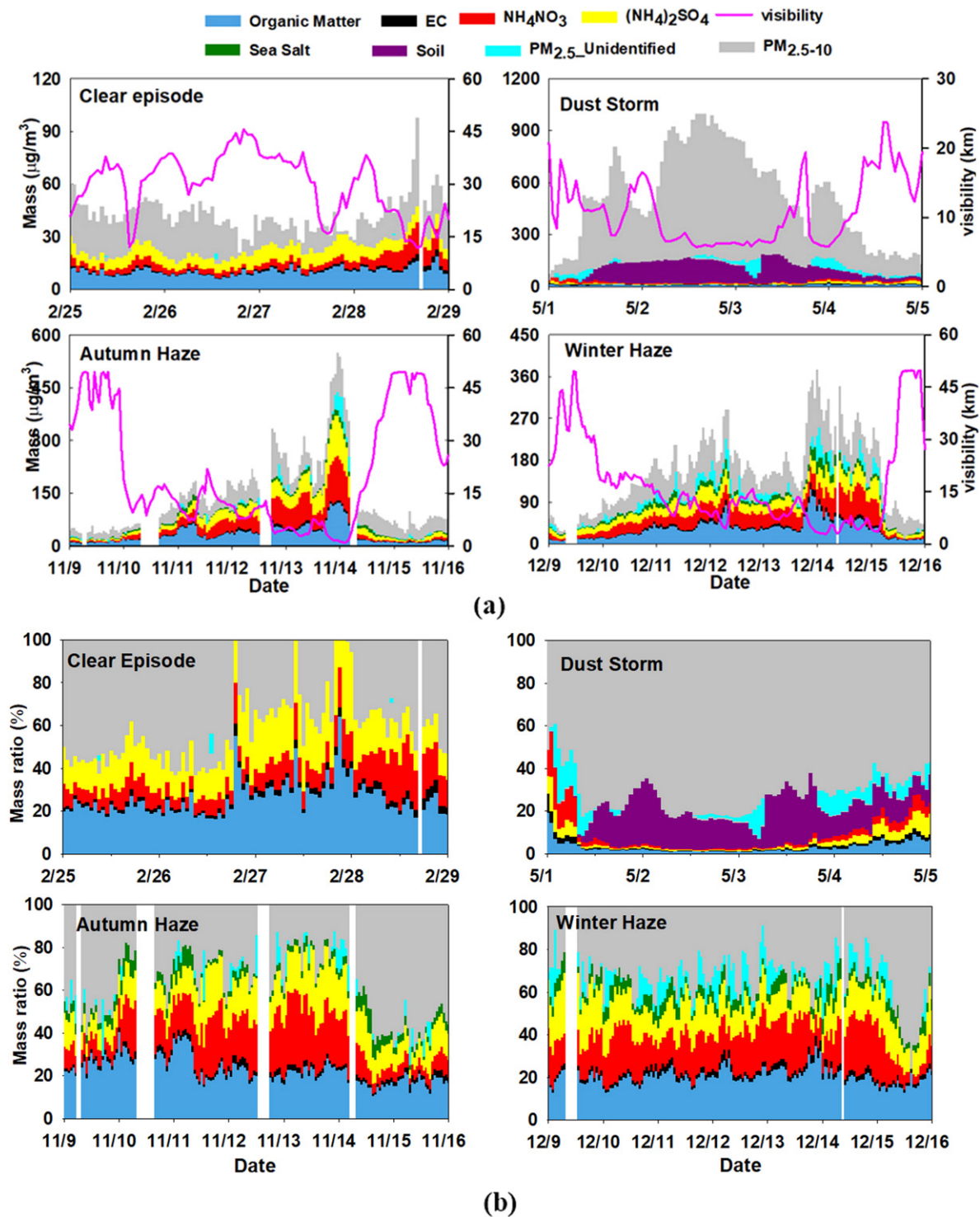


**Fig. 4.** Hourly variation of mass concentration for  $\text{PM}_{2.5}$  components, coarse particles and ambient visibility during the three low visibility events and one clear episode. (a): mass concentration and visibility. (b): mass percentage. The colour legend for each PM component: Organic Matter-Baby blue; Elemental Carbon-Black;  $\text{NH}_4\text{NO}_3$ -Red;  $(\text{NH}_4)_2\text{SO}_4$ -Yellow; Sea Salt-Dark green; Soil-Purple;  $\text{PM}_{2.5}$  Unidentified-Cyan;  $\text{PM}_{2.5-10}$ -Gray.

have no significant diversities during the clear episode, whether the absolute value or the extinction percentage. This could be explained by the stable evolution of aerosol species and relative humidity throughout the clear episode. For the event of dust storm,  $\text{PM}_{2.5}$  soil and coarse particles dominated the total extinction coefficient of  $511 \pm 150 \text{ Mm}^{-1}$  with the contributions of 16% and 46%, respectively. During the dust storm event, total extinction coefficient started to grow in synchrony with  $\text{PM}_{10}$  mass increase, and reached the maximum value of  $772 \text{ Mm}^{-1}$  at 18:00 of

May 2, 3 h later to the peak time of  $\text{PM}_{10}$  mass.  $\text{PM}_{2.5}$  soil and coarse particles contributed 17% and 63% to the maximum extinction coefficient of  $772 \text{ Mm}^{-1}$ . The sum of contributions from organic matter and secondary inorganic aerosol decreased to  $\sim 60 \text{ Mm}^{-1}$  (7%) after the dust storm arrival, then recovered to  $\sim 200 \text{ Mm}^{-1}$  (50%) after the dust storm departure. Hygroscopic enhancement could also contribute  $104 \text{ Mm}^{-1}$  (15%) around May 4 with the increased RH and inorganic components mass.

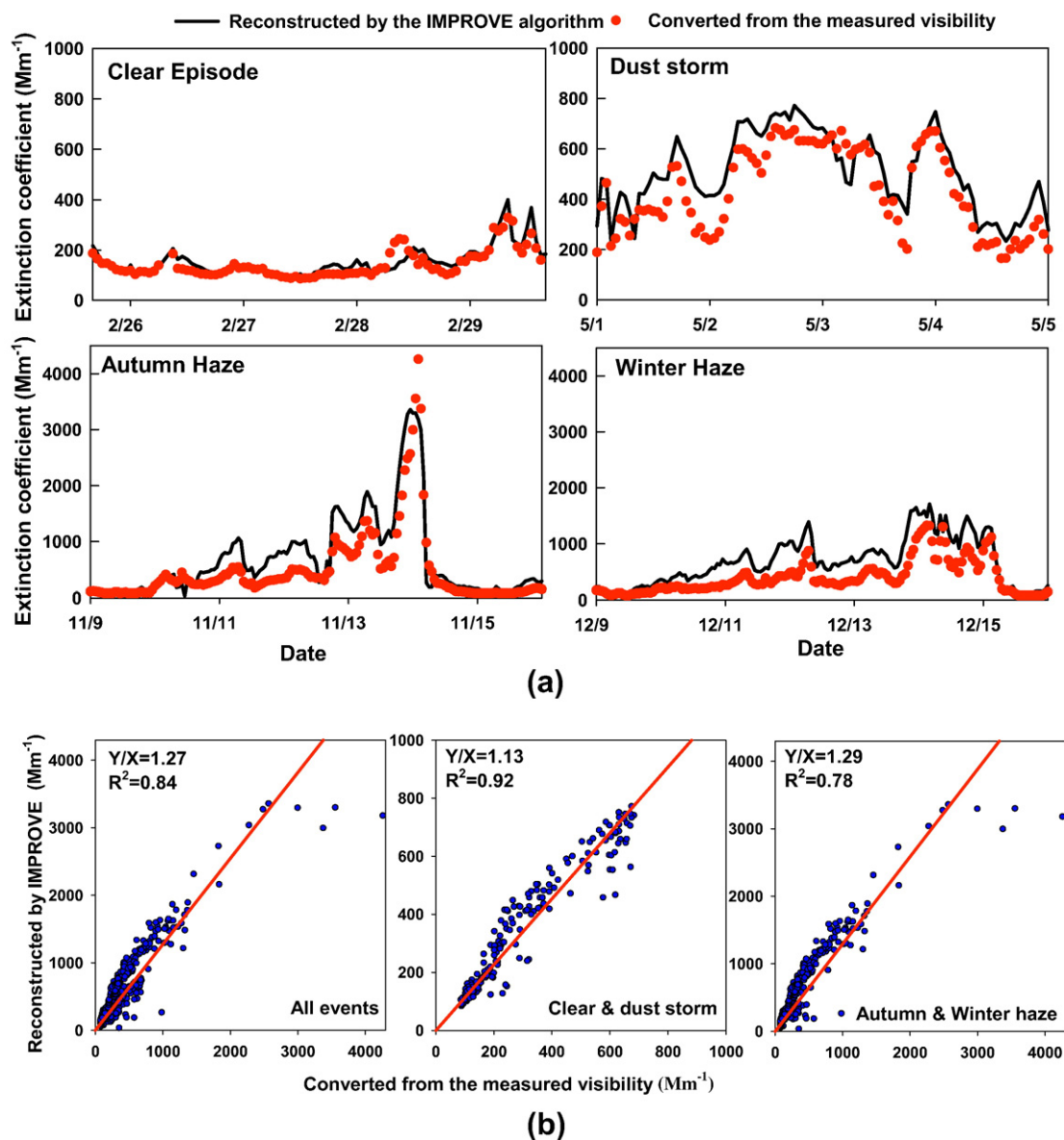
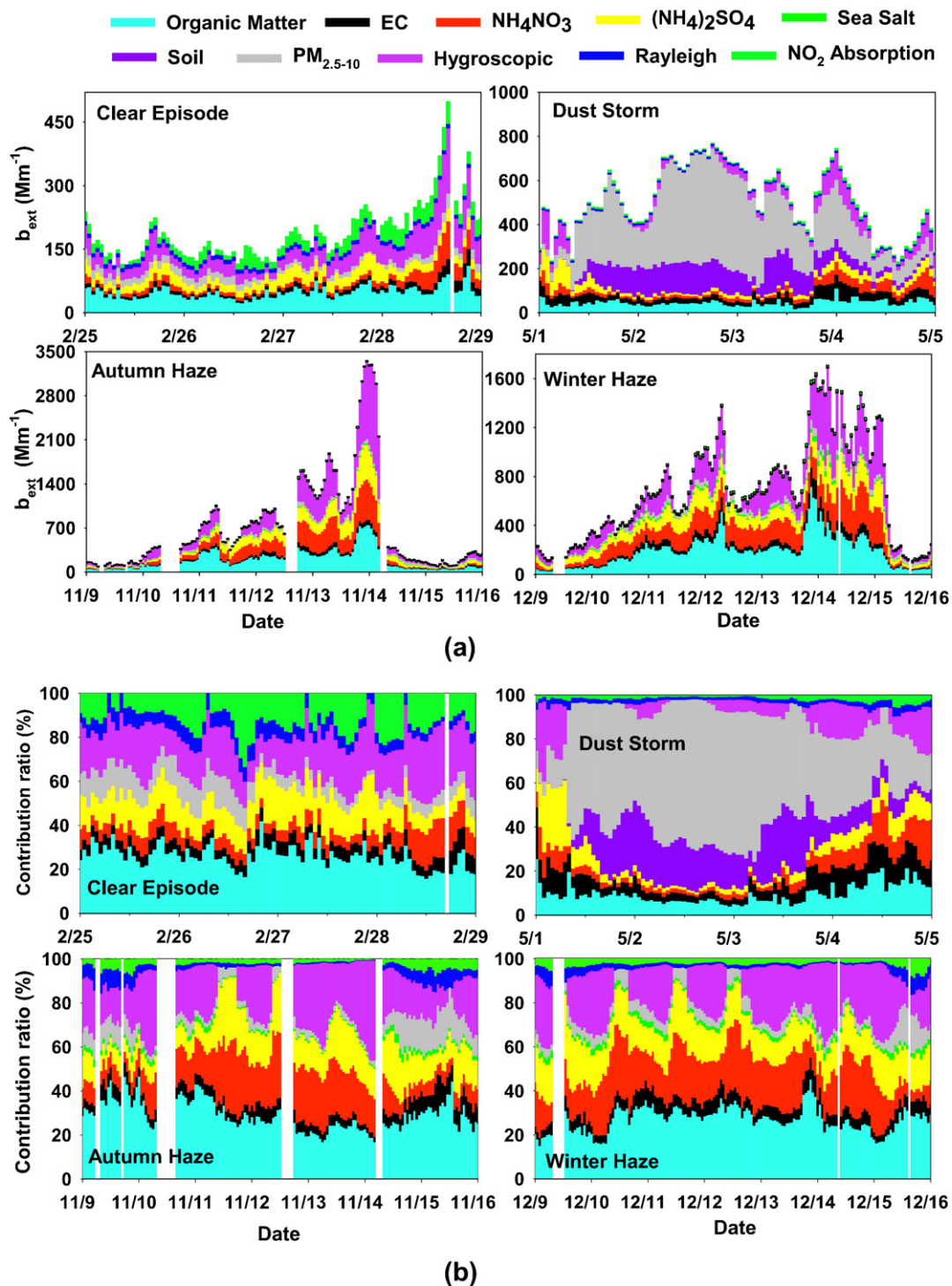


Fig. 5. Comparison of calculated extinction efficient by IMPROVE algorithm and measured values. (a) temporal distribution; (b) regression results.

For the haze events of autumn and winter, the major extinction contributors were organic matter, ammonium sulfate, ammonium nitrate and the hygroscopic enhancement of inorganic components. The average total extinction coefficient for the autumn haze and winter haze was 686 and 683 Mm<sup>-1</sup>, respectively. The major four contributions were 190–194 Mm<sup>-1</sup> (26–28%) for organic matter, 102–116 Mm<sup>-1</sup> (14–16%) for ammonium sulfate, 141–148 Mm<sup>-1</sup> (20%) for ammonium nitrate and 156–200 Mm<sup>-1</sup> (22–27%) for hygroscopic enhancement, respectively. The contribution by the coarse particles was ~4%, which was negligible in both autumn and winter events. This was also the case for that of PM<sub>2.5</sub> sea salt, Rayleigh scattering and ambient air absorption. These three contributors only accounted for 7–13 Mm<sup>-1</sup> (1–2%), 10 Mm<sup>-1</sup> (1–2%) and 9–13 Mm<sup>-1</sup> (2%), respectively during the two haze events. However, tiny differences are also identified for the extinction contributions between the autumn and winter haze events. During the autumn event, the contribution percentage of organic matter decreased from ~40% to ~20% as the event evolved, in spite of its absolute value increase from 50 to 700 Mm<sup>-1</sup>. The contribution of secondary inorganic aerosol increased from 20 to 1200 Mm<sup>-1</sup> (from 15% to 60%) as the visibility deteriorated. Correspondingly, the contribution of hygroscopic enhancement grew rapidly

from 20 to 1400 Mm<sup>-1</sup> (from 15% to 45%). During the winter event, the absolute contribution of organic matter, ammonium sulfate, ammonium nitrate and hygroscopic enhancement during the haze accumulation process increased from 46, 43, 25, 24 Mm<sup>-1</sup> to 716, 232, 353, 614 Mm<sup>-1</sup>, respectively. Their corresponding event-average contribution percentages were 27 ± 6%, 15 ± 4%, 21 ± 6% and 22 ± 8%. The low standard deviations of the contribution percentages indicated that the relative extinction contribution of various components varied in a stable and narrow range. The primary reasons for the above differences could be attributed to the more important role of inorganic species and relative humidity during the evolution of the autumn event compared to the winter event.

The evolution of chemical extinction contributions during different events had meaningful implications for the control directions towards visibility improvement. For the dust storm event, as the direct emission reduction was difficult after it has already developed, the short-term emergent procedures of coarse particles removing could be effective. For the haze events of autumn and winter, ammonium sulfate, ammonium nitrate and organic matter were the essential components for reducing the total extinction coefficient evidently. Source apportionment results of Shanghai indicated that over half of organic



**Fig. 6.** Temporal variation of extinction contribution by  $PM_{2.5}$  components, hygroscopic enhancement and coarse particle during the three low visibility events and one clear episode. (a): extinction coefficient. (b): extinction percentage. The colour legend for each PM component: Organic Matter-Baby blue; Elemental Carbon (EC)-Black;  $NH_4NO_3$ -Red;  $(NH_4)_2SO_4$ -Yellow; Sea Salt-Dark green; Soil-Purple;  $PM_{2.5-10}$ -Gray; Hygroscopic-Pink; Rayleigh-Blue;  $NO_2$  Absorption-Green.

matter was from the direct emission while the rest organic matter and SIA are all from the chemical oxidation of gaseous precursor, e.g., sulfur dioxide, nitrogen oxide and volatile organic compounds (Shanghai EPB, 2014; Zhang et al., 2012). Although Chinese government has significantly reduced emissions of sulfur dioxide in the past decade (Wang and Hao, 2012), more control efforts should be put on the control of nitrogen oxides and volatile organic compounds

in the future. Moreover, ammonium sulfate and ammonium nitrate seemed more effective than organic matter for improving the lowest visibility as of the important extinction contribution from relative humidity. The hygroscopicity are more related to inorganic aerosol (Meier et al., 2009), indicating that the mass reduction of ammonium sulfate and ammonium nitrate will weaken the extinction by itself as well as the related hygroscopic effect simultaneously.

3.4. Mass extinction efficiency of PM<sub>2.5</sub> major chemical components

The mass extinction efficiencies (MEE) are essential for the estimation of extinction contribution by each PM<sub>2.5</sub> component. It is spited to

small- and large-sized fractions according to the mass concentration for the species of organic matter, ammonium sulfate and ammonium nitrate in the revised IMPROVE algorithm. Fig. 7 shows the temporal evolution of MEEs of the three major PM<sub>2.5</sub> components as well as their

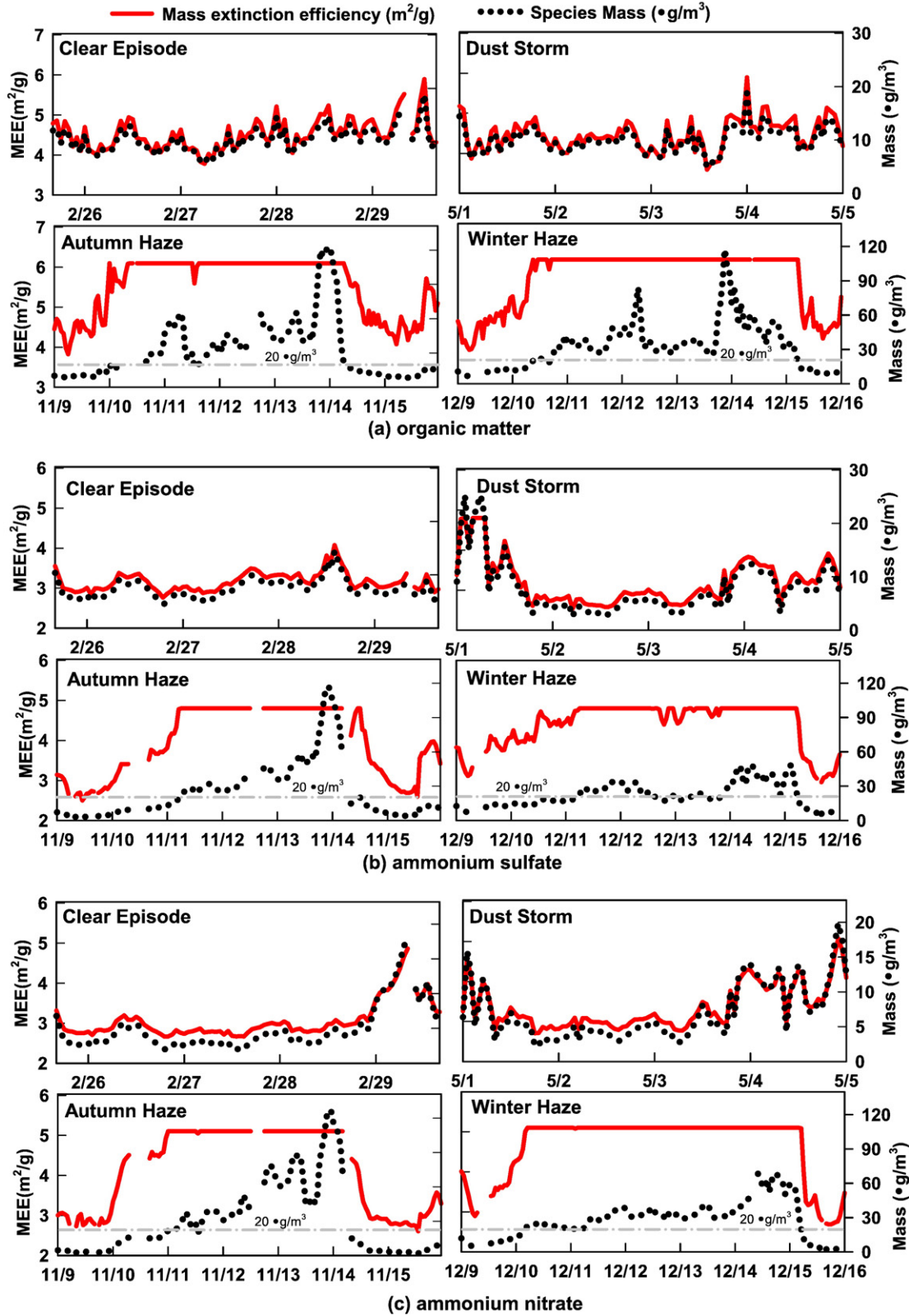


Fig. 7. Temporal evolution of mass extinction efficiency for major PM<sub>2.5</sub> compositions during the three low visibility events and one clear episode. (a) organic matter; (b) ammonium sulfate; (c) ammonium nitrate. The red solid line represents mass extinction efficiency of PM<sub>2.5</sub> components, and the black dotted line represents the mass concentration of the corresponding PM<sub>2.5</sub> components.

corresponding mass concentration during the four events. The overall variation of MEE values was similar in the events of clear episode and dust storm, in contrast to that of autumn and winter haze events.

For the species of organic matter, the MEEs during the clear episode and the dust storm event was  $4.52 \pm 0.38$  and  $4.46 \pm 0.38$ , close to the  $4 \text{ m}^2/\text{g}$  value defined in the original IMPROVE algorithm (Watson, 2002). The MEE value of autumn and winter haze event was  $5.54 \pm 0.72$  and  $5.63 \pm 0.73 \text{ m}^2/\text{g}$ , ~25% higher than that of clear episode and dust storm, mainly due to larger contributions of aged organic matter at higher mass loadings that has a higher mass extinction efficiency. The MEE results of two haze events were comparable to the large-size mode value of  $6.1 \text{ m}^2/\text{g}$  defined in the revised IMPROVE algorithm (Pitchford et al., 2007), and the review value of  $5.6 \text{ m}^2/\text{g}$  based on Mie theory (Hand and Malm, 2007), as well as the maximum value of  $6.3 \text{ m}^2/\text{g}$  measured in 2012 at the same site (Cheng et al., 2015). Meanwhile, the average MEE values of ammonium sulfate and ammonium nitrate were  $3.17 \pm 0.23$  and  $3.05 \pm 0.44 \text{ m}^2/\text{g}$  for the clear episode,  $3.21 \pm 0.57$  and  $3.35 \pm 0.54 \text{ m}^2/\text{g}$  for the dust storm event,  $3.98 \pm 0.86$  and  $4.16 \pm 1.01 \text{ m}^2/\text{g}$  for the autumn event,  $4.41 \pm 0.55$  and  $4.68 \pm 0.77 \text{ m}^2/\text{g}$  for the winter event, respectively. Similar to organic matter, the MEE value of secondary inorganic components of the two haze event were 24–38% higher than that of clear episode and dust storm. The results of clear and dust storm events were close to the value of  $3 \text{ m}^2/\text{g}$  defined in the original IMPROVE algorithm (Watson, 2002), but higher than the review results of  $2.1$ – $2.8 \text{ m}^2/\text{g}$  given by Hand and Malm (2007). The MEE values of ammonium sulfate in two haze events were close to the maximum value of  $4.7 \text{ m}^2/\text{g}$  measured in 2012 and the large-size mode values of  $4.8 \text{ m}^2/\text{g}$  (Pitchford et al., 2007; Cheng et al., 2015). Similarly, for ammonium nitrate, the MEE results in the autumn and winter events was comparable with the large-size mode values of  $5.1 \text{ m}^2/\text{g}$  in the revised IMPROVE algorithm (Pitchford et al., 2007).

The temporal evolution of MEEs during the two haze events exhibited notable different trend compared to that during the clear episode and dust storm event (presented in Fig. 7). The MEE varied proportionally to the mass of organic matter during the clear episode and dust storm event. It kept at the stable range of  $4$ – $5 \text{ m}^2/\text{g}$  throughout the clear episode. For the dust storm event, it decreased from  $5 \text{ m}^2/\text{g}$  to the minimum of  $3.6 \text{ m}^2/\text{g}$  along with the arrival of dust storm, then recovered to  $4$ – $5 \text{ m}^2/\text{g}$  when the dust storm left. During the autumn and winter haze events, the MEE value increased from  $4 \text{ m}^2/\text{g}$  at the beginning of event to the maximum of  $6.1 \text{ m}^2/\text{g}$  and remained for several days until the pollution dissipated. The maximum value of  $6.1 \text{ m}^2/\text{g}$  was equivalent to the large-size mode value of the revised IMPROVE algorithm, while the minimum value of  $3.6 \text{ m}^2/\text{g}$  was 29% higher than the small-size mode value of  $2.8 \text{ m}^2/\text{g}$  given by the revised IMPROVE algorithm. The MEE also varied proportionally to the mass of organic matter when it was lower than  $20 \mu\text{g}/\text{m}^3$ , and reached at the constant maximum value when the mass was higher than  $20 \mu\text{g}/\text{m}^3$ . The temporal trends of ammonium sulfate and ammonium nitrate MEEs were similar to that of organic matter, only with different minimum and maximum values. The corresponding minimum MEE values during the two haze events were  $2.5 \text{ m}^2/\text{g}$  for ammonium sulfate and  $2.6 \text{ m}^2/\text{g}$  for ammonium nitrate, both higher than the values of  $2.2$  and  $2.4 \text{ m}^2/\text{g}$  defined by the small-size mode values in the revised IMPROVE algorithm. The maximum values were  $4.8 \text{ m}^2/\text{g}$  for ammonium sulfate and  $5.1 \text{ m}^2/\text{g}$  for ammonium nitrate, equivalent to the large-size mode values defined in the revised IMPROVE algorithm (Pitchford et al., 2007).

The change of mass concentration for each  $\text{PM}_{2.5}$  species during the four events was the main reason for their corresponding MEE variation. According to the definition in the revised IMPROVE algorithm, the higher mass concentration of each  $\text{PM}_{2.5}$  species, the larger percentage will be attributed to the large-size mode with higher MEE value. If the component mass concentration was higher than  $20 \mu\text{g}/\text{m}^3$ , all the mass will be attributed to the large-size mode. During the peak period of the autumn and winter events, the mass concentration of the three major  $\text{PM}_{2.5}$  species were almost all larger than  $20 \mu\text{g}/\text{m}^3$  continuously,

resulting in the lasting maximum MEE value of large-size mode given by the revised IMPROVE algorithm. In contrast, during the event of clear episode and dust storm, mass loading of the above three  $\text{PM}_{2.5}$  components were all lower than  $20 \mu\text{g}/\text{m}^3$ , causing higher percentage of small-size mode with lower MEE value compared to that of haze events. It should be noted that the revised IMPROVE algorithm was developed based theoretical calculations and measurements from the U.S. IMPROVE network, whose sites are most located in pristine national parks and wilderness areas with much lower PM concentrations than those observed in this study (Pitchford et al., 2007). Therefore, the applicability of the  $20 \mu\text{g}/\text{m}^3$  threshold and two-mode design of MEEs in heavy polluted regions should be surveyed in the future. The local level of MEE for aerosol species at specific region should be investigated through the measurement of size-dependent chemical mass concentration and extinction coefficient.

#### 4. Conclusions

Three events with low visibility and one clear episode in Shanghai, China were investigated. Distinct extinction contributors were observed during their evolution.  $\text{PM}_{2.5}$  soil and coarse particles dominated the whole dust storm episode. Secondary inorganic, organic aerosol and hygroscopic enhancement by inorganic particles accounted for the autumn and winter haze events. However, the role of relative humidity expressed some differences between the autumn and winter haze events. The rapidly increased extinction coefficient during peak pollution period was not simply due to the accumulation of  $\text{PM}_{2.5}$  mass, but also related to the enhanced mass extinction efficiency of major  $\text{PM}_{2.5}$  components. Higher percentage of PM mass in the large-size mode during haze events is the basic reason for the enhancement of mass extinction efficiency. However, the cut-off value of  $20 \mu\text{g}/\text{m}^3$  for the division of small and large size in the revised IMPROVE algorithm should be investigated further in urban China according to considerable overestimate of actual extinction coefficient. All these findings will provide valuable insights about the extinction evolution towards the extreme low visibility events.

The above findings could also be expected to help to design effective control strategies towards visibility improvement. For the frequent haze events occurred in autumn and winter seasons, the effective pathway for visibility improvement seems to be the concentration reduction of organic matter and secondary inorganic aerosols. For the haze events with high relative humidity or fog mixing, control of inorganic aerosol seems more important than organic matter for a better visibility improvement, as the hygroscopic extinction contribution will be weakened along with the reduce of mass concentration for inorganic aerosol.

#### Acknowledgments

This work is supported by the National Key Research and Development Program of China (2016YFC0208700), National Natural Science Foundation of China (21625701, 21607100 & 21521064).

#### References

- Bates, T.S., Anderson, T.L., Baynard, T., Bond, T., Boucher, O., Carmichael, G., Clarke, A., Erlick, C., Guo, H., Horowitz, L., Howell, S., Kulkarni, S., Maring, H., McComiskey, A., Middlebrook, A., Noone, K., O'Dowd, C.D., Ogren, J., Penner, J., Quinn, P.K., Ravishankara, A.R., Savoie, D.L., Schwartz, S.E., Shinozuka, Y., Tang, Y., Weber, R.J., Wu, Y., 2006. Aerosol direct radiative effects over the northwest Atlantic, northwest Pacific, and north Indian oceans: estimates based on in-situ chemical and optical measurements and chemical transport modeling. *Atmos. Chem. Phys.* 6, 1657–1732.
- Bian, Q.J., 2011. Study of Visibility Degradation over the Pearl River Delta Region: Source Apportionment and Impact of Chemical Characteristics. PhD Dissertation. Division of Environment, the Hong Kong University of Science & Technology.
- Cao, J.J., Wang, Q.Y., Chow, J.C., Watson, J.G., Tie, X.X., Shen, Z.X., Wang, P., An, Z.S., 2012. Impacts of aerosol compositions on visibility impairment in Xi'an, China. *Atmos. Environ.* 59, 559–566.
- Charlson, R.J., Schwartz, S.E., Hales, J.M., Cess, R.D., Coakley, J.A., Hansen, J.E., Hofmann, D.J., 1992. Climate forcing by anthropogenic aerosols. *Science* 255, 423–430.

- Cheng, Z., Jiang, J., Chen, C., Gao, J., Wang, S., Watson, J.G., Wang, H.L., Deng, J.G., Wang, B.Y., Zhou, M., Chow, J.C., Pitchford, M.L., Hao, J.M., 2015. Estimation of aerosol mass scattering efficiencies under high mass loading: case study for the megacity of Shanghai, China. *Environ. Sci. Technol.* 49, 831–838.
- Cheng, Z., Ma, X., He, Y., Jiang, J., Wang, X., Wang, Y., Sheng, L., Hu, J., Yan, N., 2017. Mass extinction efficiency and extinction hygroscopicity of ambient PM<sub>2.5</sub> in urban China. *Environ. Res.* 156, 239–246.
- Chow, J.C., Lowenthal, D.H., Chen, L.W., Wang, X., Watson, J.G., 2015. Mass reconstruction methods for PM<sub>2.5</sub>: a review. *Air Qual. Atmos. Health* 8, 243–263.
- Fu, Q., Zhuang, G., Wang, J., Xu, C., Huang, K., Li, J., Hou, B., Lu, T., Streets, D.G., 2008. Mechanism of formation of the heaviest pollution episode ever recorded in the Yangtze River Delta, China. *Atmos. Environ.* 42, 2023–2036.
- Fu, Q., Zhuang, G., Li, J., Huang, K., Wang, Q., Zhang, R., Fu, J., Lu, T., Chen, M., Wang, Q., Chen, Y., Xu, C., Hou, B., 2010. Source, long-range transport, and characteristics of a heavy dust pollution event in Shanghai. *J. Geophys. Res. Atmos.* 115.
- Fu, X., Wang, S.X., Cheng, Z., Xing, J., Zhao, B., Wang, J.D., Hao, J.M., 2014. Source, transport and impacts of a heavy dust event in the Yangtze River Delta, China, in 2011. *Atmos. Chem. Phys.* 14, 1239–1254.
- Fu, X., Cheng, Z., Wang, S., Hua, Y., Xing, J., Hao, J.M., 2016. Local and regional contributions to fine particle pollution in winter of the Yangtze River Delta, China. *Aerosol Air Qual. Res.* 16, 1067–1080.
- Guo, S., Hu, M., Zamora, M.L., Peng, J., Shang, D., Zheng, J., Du, Z.F., Wu, Z.J., Shao, M., Zeng, L.M., Molina, M.J., Zhang, R.Y., 2014. Elucidating severe urban haze formation in China. *Proc. Natl. Acad. Sci. U. S. A.* 111, 17373–17378.
- Han, S., Bian, H., Zhang, Y., Wu, J., Wang, Y., Tie, X., Li, Y.H., Li, X.J., Yao, Q., 2012. Effect of aerosols on visibility and radiation in spring 2009 in Tianjin, China. *Aerosol Air Qual. Res.* 12, 211–217.
- Han, T., Qiao, L., Zhou, M., Qu, Y., Du, J., Liu, X., Lou, S.R., Chen, C.H., Wang, H.L., Zhang, F., Yu, Q., Wu, Q., 2015. Chemical and optical properties of aerosols and their interrelationship in winter in the megacity Shanghai of China. *J. Environ. Sci.* 27, 59–69.
- Hand, J.L., Malm, W.C., 2007. Review of aerosol mass scattering efficiencies from ground-based measurements since 1990. *J. Geophys. Res. Atmos.* 112, 321–341.
- Hua, Y., Cheng, Z., Wang, S., Jiang, J., Chen, D., Cai, S., Fu, X., Fu, Q.Y., Chen, C.H., Xu, B.Y., Yu, J.Q., 2015. Characteristics and source apportionment of PM<sub>2.5</sub> during a fall heavy haze episode in the Yangtze River Delta, China. *Atmos. Environ.* 123, 380–391.
- Huang, R.J., Zhang, Y., Bozzetti, C., Ho, K.F., Cao, J.J., Han, Y., Daellenbach, K.R., Slowik, J.G., Platt, S.M., Canonaco, F., Zotter, P., Wolf, R., Pieber, S.M., Bruns, E.A., Crippa, M., Ciarelli, G., Piazzalunga, A., Schwikowski, M., Abbaszade, G., Schnelle-Kreis, J., Zimmermann, R., An, Z.S., Szidat, S., Baltensperger, U., El Haddad, I., Prévôt, A., 2014. High secondary aerosol contribution to particulate pollution during haze events in China. *Nature* 514, 218–222.
- Jung, J., Lee, H., Kim, Y.J., Liu, X., Zhang, Y., Gu, J., Fan, S., 2009. Aerosol chemistry and the effect of aerosol water content on visibility impairment and radiative forcing in Guangzhou during the 2006 Pearl River Delta campaign. *J. Environ. Manag.* 90, 3231–3244.
- Larson, S.M., Cass, G.R., 1989. Characteristics of summer midday low-visibility events in the Los Angeles area. *Environ. Sci. Technol.* 23 (3), 281–289.
- Li, M., Zhang, L., 2014. Haze in China: current and future challenges. *Environ. Pollut.* 189, 85–86.
- Li, G.L., Zhou, M., Chen, C.H., Wang, H.L., Wang, Q., Lou, S.R., Qiao, L.P., Tang, X.B., Li, L., Huang, H.Y., Chen, M.H., Huang, C., Zhang, G.F., 2014. Characteristics of particulate matters and its chemical compositions during the dust episodes in Shanghai in spring, 2011. *Environmental Science (In Chinese)* 35, 1644–1653.
- Lin, Y., Huang, K., Zhuang, G., Fu, J. S., Wang, Q., Liu, T., Deng, C. R., Fu, Q. Y., 2014. A multi-year evolution of aerosol chemistry impacting visibility and haze formation over an Eastern Asia megacity, Shanghai. *Atmos. Environ.* 92, 76–86.
- Meier, J., Wehner, B., Massling, A., Birmili, W., 2009. Hygroscopic growth of urban aerosol particles in Beijing (China) during wintertime: a comparison of three experimental methods. *Atmos. Chem. Phys.* 9, 6865–6880.
- Pitchford, M., Maim, W., Schichtel, B., Kumar, N., Lowenthal, D., Hand, J., 2007. Revised algorithm for estimating light extinction from improve particle speciation data. *J. Air Waste Manage. Assoc.* 57, 1326–1336.
- Pui, D.Y., Chen, S.C., Zuo, Z., 2014. PM<sub>2.5</sub> in China: measurements, sources, visibility and health effects, and mitigation. *Particulology* 13, 1–26.
- Rolph, G.D., 2013. Real-time Environmental Applications and Display System (READY). <http://ready.arl.noaa.gov> (last access: 1 Oct 2016). NOAA Air Resources Laboratory, Silver Spring, MD.
- Shanghai Environmental Protection Bureau (EPB), 2014. Source Apportionment of Ambient Fine Particulate Matter for Shanghai City (Report).
- Shen, G., Xue, M., Yuan, S., Zhang, J., Zhao, Q., Li, B., Wu, H.S., Ding, A.J., 2014. Chemical compositions and reconstructed light extinction coefficients of particulate matter in a mega-city in the western Yangtze River Delta, China. *Atmos. Environ.* 83, 14–20.
- Tao, J., Cao, J.J., Zhang, R.J., Zhu, L., Zhang, T., Shi, S., Chan, C.Y., 2012. Reconstructed light extinction coefficients using chemical compositions of PM<sub>2.5</sub> in winter in Urban Guangzhou, China. *Adv. Atmos. Sci.* 29, 359–368.
- Tao, J., Zhang, L., Ho, K., Zhang, R., Lin, Z., Zhang, Z., Lin, M., Cao, J.J., Liu, S.X., Wang, G.H., 2014. Impact of PM<sub>2.5</sub> chemical compositions on aerosol light scattering in Guangzhou – the largest megacity in South China. *Atmos. Res.* 135–136, 48–58.
- Tian, M., Wang, H.B., Chen, Y., Yang, F.M., Zhang, X.H., Zou, Q., Zhang, R.Q., Ma, Y.L., He, K.B., 2016. Characteristics of aerosol pollution during heavy haze events in Suzhou, China. *Atmos. Chem. Phys.* 16, 7357–7371.
- Wang, S., Hao, J., 2012. Air quality management in China: issues, challenges, and options. *J. Environ. Sci.* 24, 2–13.
- Wang, Q., Sun, Y., Jiang, Q., Du, W., Sun, C., Fu, P., Wang, Z.F., 2015. Chemical composition of aerosol particles and light extinction apportionment before and during the heating season in Beijing, China. *J. Geophys. Res. Atmos.* 120, 12708–12722.
- Watson, J.G., 2002. Visibility: science and regulation. *J. Air Waste Manage. Assoc.* 52, 628–713.
- Zhang, H., Li, J., Ying, Q., Yu, J.Z., Wu, D., Cheng, Y., He, K.B., Jiang, J.K., 2012. Source apportionment of PM<sub>2.5</sub> nitrate and sulfate in China using a source-oriented chemical transport model. *Atmos. Environ.* 62, 228–242.
- Zhou, M., Chen, C., Wang, H., Huang, C., Su, L.Y., Chen, Y.R., Li, L., Qiao, Y.Z., Chen, M.H., Huang, H.Y., Zhang, G.F., 2012. Chemical characteristics of particulate matters during air pollution episodes in autumn of Shanghai, China. *Acta Sci. Circumst.* 32, 81–92.
- Zhou, M., Qiao, L.P., Zhu, S.H., Li, L., Lou, S.R., Wang, H.L., Tao, S.K., Huang, C., Chen, C.H., 2016a. Chemical characteristics of particulate matters and trajectory influence on air quality in Shanghai during the heavy haze episode in December, 2013. *Environ. Sci.* 37, 1179–1187.
- Zhou, M., Qiao, L., Zhu, S., Li, L., Lou, S., Wang, H., Tao, S.K., Huang, C., Chen, C.H., 2016b. Chemical characteristics of fine particles and their impact on visibility impairment in Shanghai based on a 1-year period observation. *J. Environ. Sci.* 48, 151–160.